Agronomy Research **24**(S2), xxx–ccc, 2026
https://doi.org/10.15159/AR.26.060

Spatial modeling of coffee tree height and diameter using LiDAR SLAM, RGB imagery, and field measurements

S.V. Rubio[1], G.A.S. Ferraz[1,*], E.J.S. Cardozo[1], E.H. Zavala[1], F.M. de Oliveira[1], G. Bambi[2], D. Sarri[2], G.M. Reis[3] and P.F.P. Ferraz[1]

[1]Federal University of Lavras (UFLA), School of Engineering (EENG), Department of Agricultural Engineering (DEA), Aquenta Sol, P.O. Box 3037, 37200-900 Lavras - MG, Brazil
[2]University of Florence (UniFI), Department of Agriculture, Food, Environment and Forestry (DAGRI), Via San Bonaventura, 13, IT50145 Florence, Italy
[3]Florida International University (FIU), Knight Foundation School of Computing and Information Sciences (KFSCIS), 11200 SW 8th Str, CASE 354, Miami, FL 33199, United States of America
[*]Correspondence: gabriel.ferraz@ufla.br

Received: January 30th, 2026; Accepted: July 28th, 2026; Published: August 19th, 2026

Abstract. Remote sensing has become established as a promising tool for crop management. In coffee farming, estimating canopy height and diameter is essential to characterize plant vigor, development, and uniformity. This study compared three approaches to obtain these variables: field measurements, RGB (Red, Green, Blue) imagery acquired by a Remotely Piloted Aircraft (RPA), and a handheld Light Detection and Ranging sensor (LiDAR), using geostatistics to assess spatial accuracy and agreement among methods. From three-dimensional data, surface and terrain models were derived, enabling estimation of canopy height and diameter, while geostatistics was used to characterize the spatial structure, select variogram models via cross-validation, and generate continuous maps through ordinary kriging. In pointwise comparison with field data, LiDAR showed better performance for height (R^2 = 0.80) than the RGB orthomosaic (R^2 = 0.63). For canopy diameter, LiDAR was also superior (R^2 = 0.79) relative to RGB imagery (R^2 = 0.71). At the spatial level, the comparison between kriged maps indicated greater agreement between LiDAR and field data, especially for plant height (r = 0.99), whereas RGB and field data showed lower spatial correspondence (r = 0.44). For canopy diameter, the maps derived from LiDAR and RGB showed good agreement with field data, with r = 0.88 and r = 0.83, respectively. Thus, the combination of pointwise assessment and geostatistical analysis proved suitable for comparing the studied methods and for interpreting, in an integrated manner, the estimation and spatial distribution of coffee tree height and canopy diameter.

Key words: digital and precision agriculture, morphometric modeling, point cloud, spatial interpolation, precision phenotyping.

INTRODUCTION

Coffee is a strategic agro-industrial activity on a global scale and is particularly relevant for Brazil due to its production weight and its role in foreign trade. Between January and October 2025, Brazil exported 34.2 million bags and, due to the increase in international prices, the export value reached in October 2025 the highest monthly record since 1997 (US$ 1.6 billion) (Conab, 2025). Globally, coffee is produced in about 60 countries and represents a key source of income for many economies, with Brazil among the main producers (Santana et al., 2021b). In this context, crop monitoring is essential because coffee farming exhibits spatial and temporal variability in soil–plant system attributes that condition its performance; therefore, precision coffee farming seeks to optimize inputs and management decisions as a function of this variability (Santana et al., 2021b).

Among coffee tree attributes, canopy height and canopy diameter are biophysical parameters used to describe growth and development and, therefore, have been employed in the temporal monitoring of cultivars under field conditions (Bento et al., 2022). In addition, these structural traits are sensitive to water and nutritional conditions and may act as early indicators associated with crop performance (Silva et al., 2025). However, manual surveying can be difficult in large areas (Bento et al., 2022) and may introduce errors due to tape inclination and the architecture of branches and leaves (Barbosa et al., 2021a). For this reason, the literature has driven alternative approaches for measurements that are difficult to carry out with conventional tools (Bento et al., 2023).

In this context, RPAs equipped with RGB cameras and processed by Structure from Motion (SfM) allow the reconstruction of 3D point clouds and the generation of a Digital Surface Model (DSM) and a Digital Terrain Model (DTM); from their difference, the Canopy Height Model (CHM) is obtained to derive structural variables in coffee plantations (Santos et al., 2020; Barbosa et al., 2021b; Martello et al., 2022). This workflow has been applied in recurrent monitoring schemes, using ground control points to qualify georeferencing, followed by height extraction via DSM–DTM and canopy diameter extraction from the orthomosaic (Santos et al., 2020). In multitemporal approaches, successive campaigns have been used to capture the spatial and temporal variability of coffee trees, including individual plant delineation to obtain plant-level metrics (Martello et al., 2022). Complementarily, there are studies that prioritize monitoring using vegetation indices derived from RGB images, incorporating point-cloud quality control procedures such as outlier removal (Barbosa et al., 2021b).

LiDAR is an active remote sensing sensor that uses a laser to measure distances and, thus, capture the three-dimensional structure of the canopy, standing out for its adaptability to different environmental conditions (Wang et al., 2021; Mora-Pérez et al., 2025). In coffee fields, the use of airborne LiDAR on an RPA (DJI Zenmuse L1) enabled the estimation of canopy height and diameter from digital models (DSM/DTM) at different resolutions, through longitudinal and transverse profiles (Mora-Pérez et al., 2025). In fruit crops, Wang et al. (2021) developed a Mobile Laser Scanning (MLS) system based on Simultaneous Localization and Mapping (SLAM) to reconstruct point clouds in orchards, segment canopies, and obtain morphological parameters.

Geostatistics provides a robust framework to describe and map spatial variability through semivariogram fitting (e.g., spherical, exponential, or gaussian models) and interpolation by ordinary kriging, generating continuous surfaces from point sampling (Abreu et al., 2024; Quispe et al., 2025). This approach relies on parameters such as nugget effect, sill, and range, which quantify autocorrelation and allow classification of the degree of spatial dependence, while also supporting sampling decisions and the delineation of management units (Ferraz et al., 2017; Maita et al., 2025). In coffee crops, it has been applied to quantify the spatial structure of plant attributes (including canopy height and diameter) and their spatial dependence, enabling thematic maps representative of field distribution (Carvalho et al., 2013; Ferraz et al., 2017). In addition, it has been used to model the spatial variability of yield and its relationship with foliar nutritional status, through variograms and kriging-based mapping (Silva et al., 2013). In other systems, its usefulness has been reported for dendrometry and soil parameters, with model selection via cross-validation and generation of kriged maps (Grego et al., 2010; Almeida et al., 2016; Cortes et al., 2023; Yu et al., 2024).

Although several studies have compared LiDAR and RGB–SfM to estimate structural variables (e.g., height and canopy metrics), they generally assess performance using point-based metrics and bias analysis between methods, without integrating geostatistics to verify whether both sources consistently reproduce the crop's spatial structure beyond point accuracy. For example, systematic differences between SfM and LiDAR products have been documented when extracting height and canopy projection (Bing et al., 2025), comparisons in coffee plantations using LiDAR and RGB/SfM point clouds for height (Bento et al., 2025), and evaluations in woody crops with RGB images from RPA versus MLS data (Escolà et al., 2023; Torres-Sánchez et al., 2023), as well as analyses at the individual-tree level (You et al., 2023). In contrast, Yu et al. (2024) explicitly integrated geostatistics with LiDAR to analyze spatial effects of canopy cover in natural forests, but not as a LiDAR–RGB comparative framework, which highlights the opportunity to incorporate this analysis to contrast patterns, scales of variation, and spatial agreement between maps, strengthening site-specific decisions.

Given this scenario, the objective of this study is to compare the estimation of canopy height and diameter in coffee using three approaches (manual measurement, three-dimensional reconstruction from RGB images, and handheld LiDAR with SLAM technology) and to integrate geostatistics to assess both accuracy and spatial coherence among methods. The main contribution is to provide a comparative assessment, within the same experimental unit, that combines agreement metrics and spatial mapping to identify the potentialities and limitations of each data source.

MATERIALS AND METHODS

Study area

The experiment was conducted in an arabica coffee plantation (*Coffea arabica L.*), located at the Federal University of Lavras (UFLA), in the municipality of Lavras, Minas Gerais, Brazil (21°13′30.1″ S; 44°58′14.9″ W), at 930 m altitude (Fig. 1). The study area comprises approximately 0.15 hectares and is composed of 2-year-old coffee trees, arranged in planting rows with a spacing of 3.5 m between rows and 0.7 m between plants.

Field data acquisition

The sampling design was defined by systematic sampling, totaling 33 sampling points distributed across two coffee rows (Fig. 1). The shortest distance between points was approximately 4 m, whereas the longest distance was approximately 113 m. Reference field measurements were collected on November 20, 2025, using a measuring tape, and served as the standard for evaluating the remote sensing–based methods.

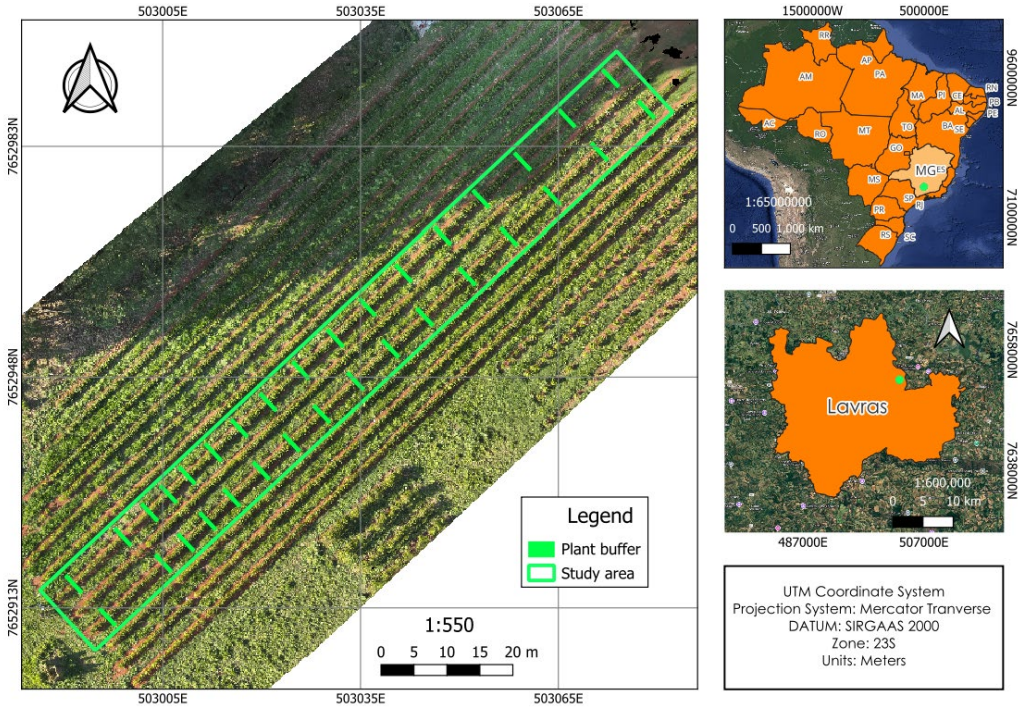

Figure 1. Location of the study area and sampling points.

According to the Köppen climate classification, the region has a humid subtropical climate with monsoon influence (*Cwa*), characterized by a dry winter and a rainy summer (Álvares et al., 2013; Santos et al., 2023). The average annual precipitation is 1,460 mm and the average annual temperature is 20.4 °C (Dantas et al., 2007).

Plant height was defined as the vertical distance between the ground and the top of the canopy, disregarding small branches projecting above the main structure, as they were treated as outliers. Canopy diameter was measured at the mid-third of each plant as the distance transverse to the crop row (perpendicular to the direction of the rows). In all measurements, outlier branches were disregarded, defined as small branches identified by the operator that grow outside the main canopy direction, interfering with a representative morphological delineation of the plant (Barbosa et al., 2021a).

Georeferencing of the sampling points was performed using the RPA equipped with Real-Time Kinematics (RTK). To ensure unambiguous identification of each plant in the image, white sheets were placed next to the sampled plants, serving as visual markers.

RGB image acquisition

Image acquisition was carried out on the same day as the reference field measurements, using a DJI Mavic 3T Enterprise multirotor RPA (SZ DJI Technology Co., Ltd, Shenzhen, China). The platform integrates a set of onboard sensors consisting of a wide-angle camera in the visible spectrum (red, R; green, G; and blue, B bands), a telecamera, and a Long-Wave Infrared (LWIR) thermal camera, enabling rapid switching between acquisition modes and detailed target observation (DJI, 2022).

Although the equipment is widely used in thermal applications, this study exclusively used the RGB images obtained by the wide-angle camera. According to the manufacturer's specifications, the wide-angle camera of the Mavic 3T/3TA features a 1/2" CMOS sensor with 48 MP and a 24 mm equivalent lens (84° FOV; f/2.8 aperture), while the telecamera uses a 1/2" CMOS sensor, 12 MP, f/4.4 aperture, and hybrid zoom up to 56×. The onboard thermal camera has a resolution of 640×512 and modes with indicated measurement ranges of −20 to 150 °C (high gain) and 0 to 500 °C (low gain; theoretical value) (DJI, 2022).

Flights were conducted at 30 m altitude, with a speed of 5 m s^{-1} and 80% overlap. To ensure higher positional accuracy, the system was operated with RTK, using the RTK module attached to the PSDK port together with the DJI D-RTK 2 mobile GNSS station (SZ DJI Technology Co., Ltd, Shenzhen, China), waiting for the 'FIX' status before data collection.

LiDAR data acquisition

The survey was carried out with the GS-100G MLS (Wuhan Geosun Navigation Technology Co., Ltd, Wuhan, China), a handheld laser scanning system that integrates a Global Navigation Satellite System (GNSS), Inertial Navigation System (INS), LiDAR, and SLAM algorithms for continuous acquisition in outdoor and indoor environments. The equipment operates with a 360° (horizontal) × 270° (vertical) field of view, 16 channels, and an acquisition rate of up to 320,000 points s^{-1} (single return) or 640,000 points s^{-1} (dual return). The reported range is 80 m (10% reflectance), with a maximum range of 120 m, and a distance accuracy of ± 1.5 cm. It has a point-cloud accuracy of 5 cm at 100 m (without a control point) and a mass of 1.7 kg (without battery), characteristics that favor manual operation and rapid acquisition in agricultural plots (Geosun, 2022a).

To reduce drift inherent to SLAM uncertainties, scanning trajectories were planned considering route length and duration, as well as the presence of stable structural elements that act as geometric 'anchors', contributing to the consistency of the point cloud throughout the survey (Pereira-Obaya et al., 2024). The SLAM trajectory closure error was 1.079 m, equivalent to 0.406% of the total path length traveled (265.91 m).

RGB image processing

Following the methodology described by Bento et al. (2025), the RGB images acquired by RPA were processed in Pix4D Mapper (version 4.5.6) using an SfM-based photogrammetric workflow. First, automatic calibration and alignment (aero triangulation) were performed, in which the software identifies homologous points between overlapping images and estimates the camera's internal orientation and the external orientation of each photograph, generating a sparse point cloud as an initial solution. Subsequently, the reconstruction was densified to increase the number of 3D

points and reduce gaps, refining the canopy representation. Finally, the images were orthorectified and the outputs generated included the point cloud, the RGB orthomosaic, and the DTM and DSM digital elevation models.

LiDAR data processing

LiDAR data were initially processed in PointCloudCreater (version 2.0.46) (Geosun, 2022b) to generate point clouds in LAS format. Next, the LiDAR cloud was co-registered to the cloud derived from RGB images to ensure geometric consistency between sources before extracting structural metrics, with a co-registration root mean square error (RMSE) of 0.205 m. After spatial clipping to the perimeter of the study area, noise removal was performed in CloudCompare (version 2.14.beta) using the Statistical Outlier Removal (SOR) filter, following the procedure of Pinedo et al. (2025): the global mean distance and the standard deviation of distances to the k nearest neighbors were estimated; then, a threshold value was defined by adding to the global mean a number of standard deviations proportional to parameter m, removing as outliers the points that exceeded this threshold, with $k = 8$ and $m = 30$. Next, ground classification was performed via Cloth Simulation Filtering (CSF) (Zhang et al., 2016), implemented in the lidR package (R version 4.5.2), with 0.5 m resolution, 500 maximum iterations, and a 0.1 m classification threshold. After classification, the empirical point densities were 2,741.85 points m^{-2} for the ground class and 6,804.59 points m^{-2} for the vegetation class. Finally, the ground-classified cloud was rasterized at 2 cm resolution to generate the DTM, while the full cloud was rasterized at the same resolution to compose the DSM. In both steps, the Triangulated Irregular Network (TIN) algorithm was used, which interpolates the surface from a mesh of triangles formed by neighboring points.

Extraction and evaluation of structural variables

The extraction of structural variables was performed in QGIS software (version 3.44.6) (QGIS Development Team, Open Source Geospatial Foundation). Initially, the CHM was obtained by subtracting the DTM from the DSM using the Raster Calculator. Then, using the CHMs derived from LiDAR and RGB images, plant height and canopy diameter were estimated based on the procedure described by Mora-Pérez et al. (2025), employing the Elevation Profile tool. For each sampling point, a single transverse profile was drawn across the planting row, as illustrated in Fig. 2. To reduce observer dependence, the profiles were standardized in terms of position, orientation, and dimensions, being drawn perpendicular to the row, centered on the sampling point of the evaluated plant, with a transverse length of 2 m and a width of 0.25 m. The same profile line was applied to the CHMs derived from LiDAR and RGB, allowing direct comparison between methods. Height was defined as the highest altimetric peak representative of the canopy in each CHM. Canopy diameter was measured as the maximum transverse distance of the continuous segment associated with the main canopy, disregarding isolated peaks or projected branches outside the main canopy outline.

Accuracy assessment was performed by comparing plant height and canopy diameter estimates obtained from LiDAR and the RGB sensor with the respective reference values measured in the field. For each variable, the correlation between methods was analyzed and a linear model was fitted between the estimates and the reference values. Performance was quantified using the coefficient of determination (R^2),

Pearson correlation (r), Root Mean Square Error (RMSE), and Mean Error (ME), allowing evaluation of fit, error magnitude, and systematic bias. Additionally, paired comparisons between methods were performed for each structural variable. For this purpose, the normality of the paired differences was verified using the Shapiro–Wilk test, adopting a 5% significance level. When the differences showed a normal distribution ($p > 0.05$), the paired t-test was applied; when this assumption was not met, the Wilcoxon signed-rank test was used. In both cases, significant differences were considered at the 5% level ($p < 0.05$).

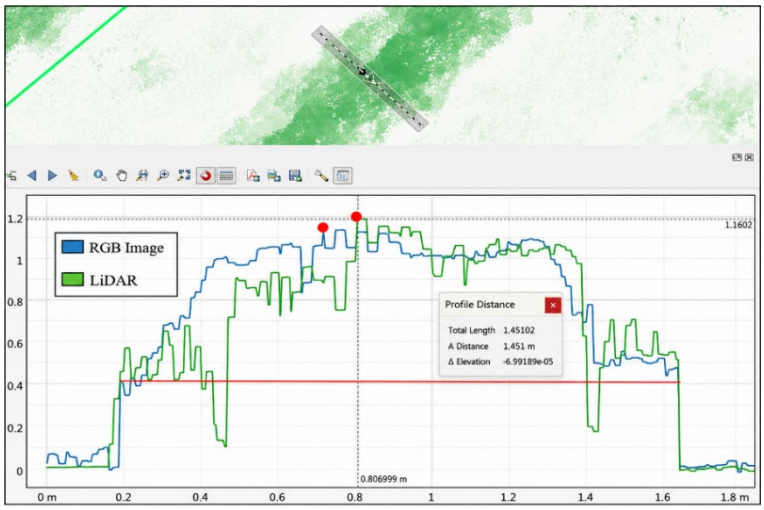

Figure 2. Transverse profile across the planting row to measure plant height and canopy diameter.

Geostatistical analysis and map generation

Geostatistical analysis was conducted in R Development Core Team, version 4.5.2 (2025), using the geoR package (Ribeiro Junior & Diggle, 2001), with the aim of modeling the spatial variability of plant height and canopy diameter. The methodological sequence described by Scalon (2024) was followed, including: (i) exploratory analysis, (ii) modeling spatial dependence through semivariograms, and (iii) kriging interpolation, generating prediction and standard-error maps.

Exploratory analysis was used to characterize the data distribution, check for the presence of outliers, and support the initial interpretation of the evaluated variables. Subsequently, spatial dependence was assessed using experimental semivariograms calculated with the Matheron (1962) estimator (Eq. 1). Considering the reduced number of sampling points, restricted maximum likelihood (REML) estimation was adopted, since estimators based on the method of moments may show limited performance in variogram estimation for datasets with fewer than 100 points (Webster & Oliver, 2007). Under this sampling condition, the use of REML is recommended, as it tends to produce less biased estimates of variance parameters in small samples (Diggle & Ribeiro Jr., 2007; Kerry & Oliver, 2007). The method, originally proposed by Patterson & Thompson (1971), is based on linear combinations of the data, allowing random and deterministic components of variation to be estimated simultaneously, thereby reducing bias in parameter estimation (Marchant & Lark, 2007; Ferraz et al., 2012).

Theoretical spherical, exponential, and gaussian models were subsequently fitted to estimate the nugget effect (C_0), contribution (C_1), sill ($C_0 + C_1$), range (A), and practical range (A'). To assess the uncertainty associated with the fitted parameters, 95% confidence intervals were estimated using a jackknife procedure, in which the sampling points were removed individually and the models were refitted. Model selection was performed using leave-one-out cross-validation (LOOCV), using RMSE and the Degree of Spatial Dependence (DSD) as criteria. DSD was calculated as the ratio between the nugget effect and the sill, classified according to Cambardella et al. (1994), which considers dependence strong when the nugget effect represents less than 25% of the sill, moderate between 25% and 75%, and weak above 75%.

$$\gamma(h) = \frac{1}{2N(h)} \sum_{i=1}^{N(h)} [Z(X_i) - Z(X_i + h)]^2 \quad (1)$$

where $\gamma(h)$ is the semivariogram; $N(h)$ is the number of experimental pairs of observations $Z(X_i)$ and $Z(X_i + h)$ separated by a distance h; Z can be any of the studied attributes; X_i is the georeferenced position at which the variable (attribute) Z occurred.

After semivariogram fitting, the variables were interpolated by ordinary kriging to represent, in maps, the spatial distribution patterns of the crop's structural attributes, adopting a spatial resolution of 5 cm. In addition, kriging prediction standard-error maps were generated, which express the standard deviation associated with the estimate at each location and provide a measure of the reliability of the interpolated values in the study area (Ferraz et al., 2017).

The maps produced for each variable and for each data acquisition method were compared using metrics calculated from pixel-wise differences between the kriged surfaces. In this step, Pearson's correlation coefficient (r), Mean Error (ME), and Root Mean Square Error (RMSE) were used, considering the comparisons between RGB and field data, LiDAR and field data, and LiDAR and RGB. In addition, the agreement among methods was complemented by a predictive cross-validation approach based on LOOCV. For this analysis, ME and RMSE were calculated at the excluded locations, allowing the predictive performance of the methods to be assessed beyond the direct comparison between kriged surfaces.

RESULTS AND DISCUSSION

Descriptive statistics of the coffee tree structural variables obtained by the two evaluated sensors (RGB and LiDAR) and by field measurements are presented in Table 1, showing close agreement among the estimated values. Regarding variability, the Coefficients of Variation (CV) indicate moderate behavior (10–20%), according to the classification of Gomes & Garcia (2002), whereas values below 10% are considered low and associated with greater homogeneity. In this context, LiDAR showed a moderate CV for height (10.63%) and diameter (12.71%), while RGB exhibited higher moderate CVs (18.06% and 15.01%). Therefore, because higher CVs constitute an initial indication of data heterogeneity (Frogbrook et al., 2002), the larger CVs observed for RGB suggest greater internal variability in the estimates derived from this sensor.

Table 1. Descriptive statistics of coffee plant height and canopy diameter obtained from field measurements, RGB imagery, and handheld LiDAR

Variable	Min. (cm)	Max. (cm)	Mean (cm)	Median (cm)	1st Quar. (cm)	3rd Quar. (cm)	Variance (cm^2)	Standard Deviation (cm)	CV (%)
Field height	78.00	132.0	113.4	118.0	105.0	122.0	183.6	13.55	11.95
RGB height	63.80	135.6	105.6	109.9	100.3	116.8	363.5	19.06	18.06
LiDAR height	85.51	134.8	109.4	111.0	100.7	116.8	135.3	11.63	10.63
Field canopy diameter	92.00	156.0	129.3	134.0	118.0	142.0	305.2	17.47	13.51
dGB canopy diameter	65.06	160.0	131.0	133.7	122.7	143.6	386.8	19.67	15.01
LiDAR canopy diameter	90.88	158.1	130.1	132.8	117.2	140.8	273.3	16.53	12.71

Linear regressions show that canopy height and diameter estimates had a positive association with field data (Fig. 3, a, b, c, d). For height, handheld LiDAR showed greater agreement with the field than RGB imagery. This behavior is consistent with Mora-Pérez et al. (2025), who estimated coffee tree height and diameter from the CHM generated with airborne laser scanning (ALS), extracting metrics using transverse profiles. For height, the authors reported R^2 between 0.8382 and 0.8554 with the profile-based approach (depending on resolution), values close to that obtained in this study with handheld LiDAR. For diameter, Mora-Pérez et al. (2025) observed R^2 between 0.8763 and 0.9610, higher than observed here ($R^2 = 0.7951$), suggesting better diameter agreement when derived from ALS products, although under a distinct acquisition configuration. However, this comparison has a methodological character and is not directly equivalent, since the cited study used ALS, with different point density and spatial resolution compared with the handheld system employed in the present study.

For diameter, the results using RGB imagery ($R^2 = 0.7116$, $r = 0.8435$, RMSE = 10.577 cm) were below the performance reported in coffee by Santos et al. (2020), who observed $R^2 \geq 0.78$ across months and RMSE errors of 0.08 m for diameter and 0.06 m for height, and by Bento et al. (2022), who reported $r = 0.934$ and RMSE = 8.54 cm for diameter and $r = 0.885$ and RMSE = 9.07 cm for height. In the comparison between handheld LiDAR and RGB imagery, moderate agreement was observed for height (Fig. 3, e: $R^2 = 0.5054$, $r = 0.7109$) and higher agreement for diameter (Fig. 3, f: $R^2 = 0.6904$, $r = 0.8309$), in contrast with Bento et al. (2025), who reported height between sensors of $R^2 = 0.72$ and $r = 0.85$. The pointwise performance metrics for all combinations between the evaluated methods and variables are presented in Table 2.

Discrepancies between sensors can be interpreted based on evidence obtained with handheld LiDAR in agricultural systems. Escolà et al. (2023) showed that the LiDAR point cloud has a point density about three times higher than that obtained from RGB imagery and captures the variability of the canopy top and sides in greater detail, although it can be affected by occlusions, mixed pixels, and understory vegetation. Similarly, Torres-Sánchez et al. (2023) observed high correlation between both sources (R^2 from 0.82 to 0.94), with improvement in longer sections, and indicated that geometric parameters estimated by handheld LiDAR tend to be systematically higher than those derived from photogrammetry.

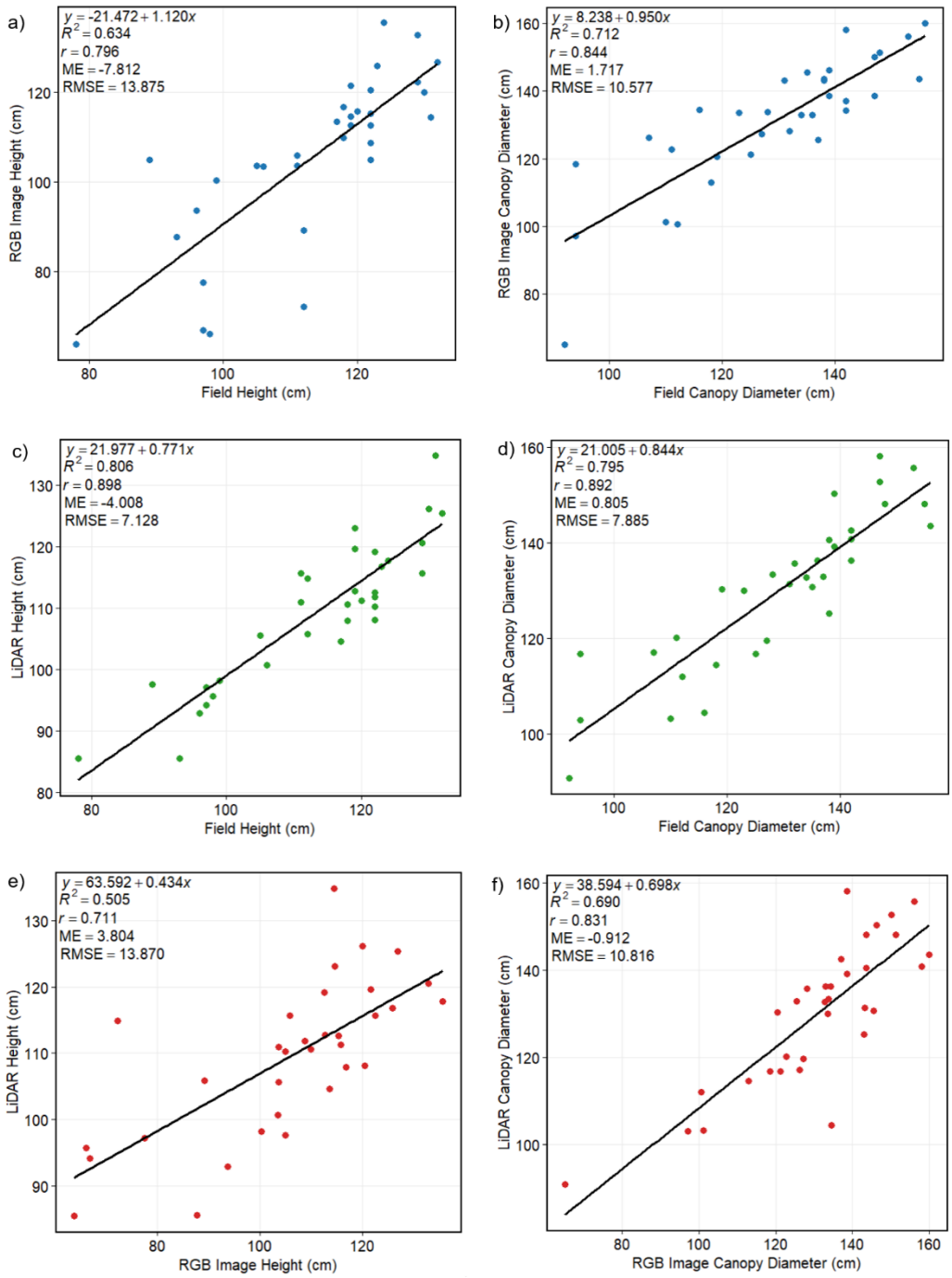

Figure 3. Linear regressions between estimates of: a) plant height from RGB imagery and field data, b) canopy diameter from RGB imagery and field data, c) plant height from LiDAR data and field data, d) canopy diameter from LiDAR data and field data, e) plant height from LiDAR data and RGB imagery, and f) canopy diameter from LiDAR data and RGB imagery.

These aspects help explain both the stronger alignment of LiDAR with field data and the lower agreement between LiDAR and RGB, especially when image-based reconstruction is more sensitive to occlusions and to the definition of the effective canopy outline. However, this comparison incorporates the uncertainty of the adopted manual reference, since the field measurements were performed using a measuring tape, a method whose precision may be lower than the nominal precision of sensors such as LiDAR.

Table 2. Summary of pointwise agreement metrics among field, RGB and LiDAR estimates for plant height and canopy diameter

Comparison	Variable	R^2	r	ME (cm)	RMSE (cm)
RGB image vs. Field	Plant height	0.6343	0.7964	-7.812	13.875
RGB image vs. Field	Canopy diameter	0.7116	0.8435	1.717	10.577
LiDAR vs. Field	Plant height	0.8065	0.898	-4.008	7.128
LiDAR vs. Field	Canopy diameter	0.7951	0.8917	0.8045	7.885
LiDAR vs. RGB image	Plant height	0.5054	0.7109	3.804	13.870
LiDAR vs. RGB image	Canopy diameter	0.6904	0.8309	-0.9121	10.816

On the other hand, previous studies on coffee plants indicate that RGB images obtained using RPAs can also generate consistent estimates of plant height and canopy diameter when associated with ground control points (GCPs), demonstrating that this strategy is feasible under conditions in which RTK-equipped platforms are not available (Santos et al., 2020; Santana et al., 2021a; Barbosa et al., 2021b). However, the reliability of these products depends directly on the quality of the georeferencing. Sanz-Ablanedo et al. (2018) demonstrated that the accuracy of SfM photogrammetry is influenced by the number and location of GCPs, recommending their uniform distribution throughout the entire area of interest, ideally in a triangular mesh, to minimize the maximum distance to the nearest control point. The authors also indicated that, for the same number of GCPs, an optimal distribution can double the accuracy compared with poorly distributed configurations.

In addition to georeferencing, the characteristics of the RGB camera may also influence the results obtained through photogrammetry. The DJI Mavic 3T was used because it was available at the time of the experiment and allowed RGB images to be obtained with RTK support. However, because it has a 1/2" CMOS sensor, which is smaller than those of other platforms designed for specialized mapping, this configuration may have partially contributed to the lower performance of the estimates derived from RGB images. Even so, previous studies on coffee plants have obtained favorable results using small-format sensors, such as the Sony EXMOR 1/2.3" sensor mounted on a DJI Phantom 3 Professional (Santos et al., 2020; Barbosa et al., 2021a; Barbosa et al., 2021b).

The proximity between the field data and the estimates obtained from RGB and LiDAR was complemented by paired tests between methods (Fig. 4). For plant height, statistically significant differences were observed between field and RGB (Fig. 4, a) and between field and LiDAR (Fig. 4, c), indicating systematic deviations in relation to the manual reference. This result partially differs from Bento et al. (2022), who did not observe significant differences between field measurements and aerial images for plant height and canopy diameter in coffee plants. In the present study, this equivalence occurred only for canopy diameter, with no significant differences between field and RGB (Fig. 4, b) or between field and LiDAR (Fig. 4, d). Between sensors, no significant

differences were observed for height (Fig. 4, e) or diameter (Fig. 4, f), a result similar to that reported by Bento et al. (2025).

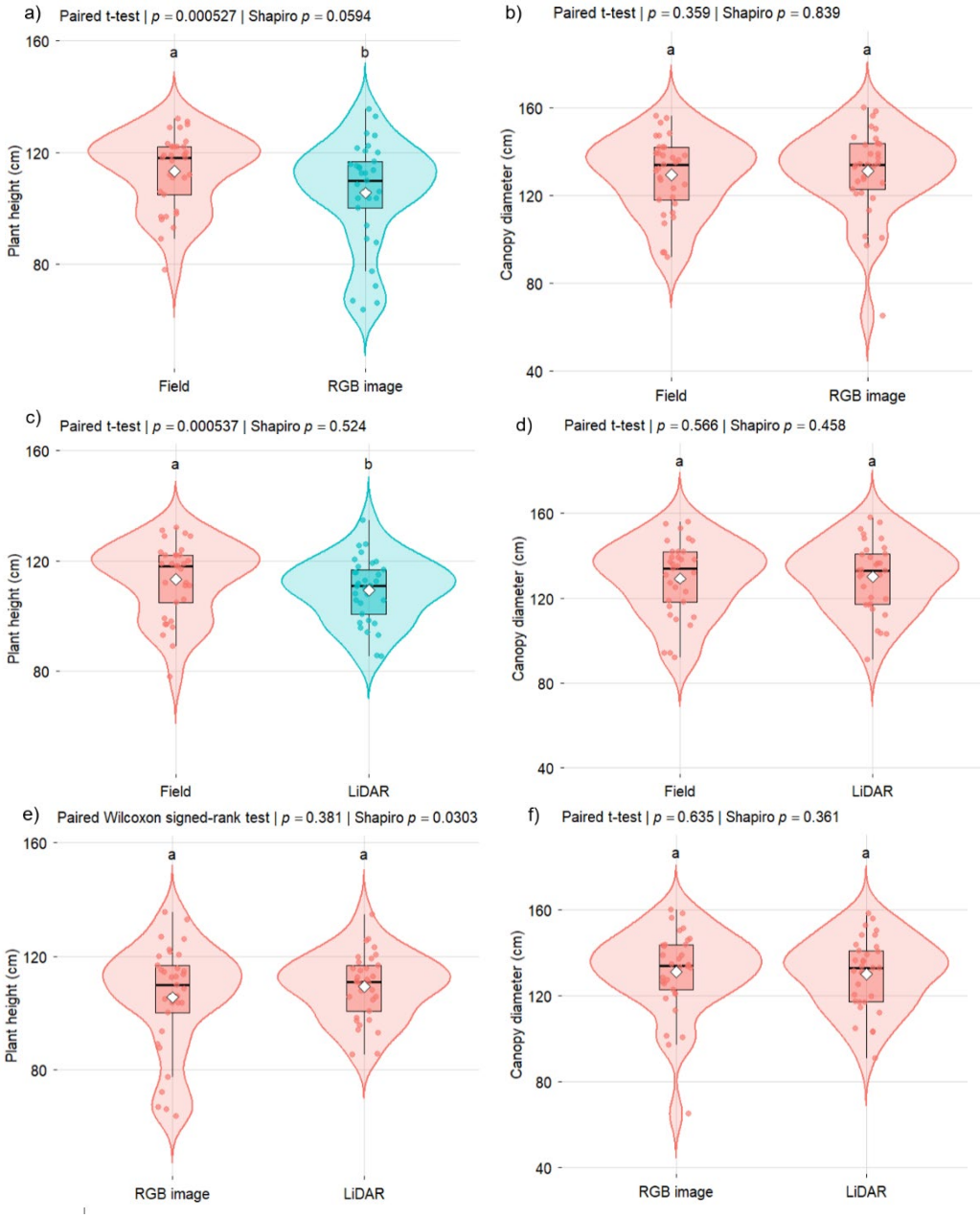

Figure 4. Distribution of values and results of the paired tests for: a) plant height between RGB images and field data, b) canopy diameter between RGB images and field data, c) plant height between LiDAR data and field data, d) canopy diameter between LiDAR data and field data, e) plant height between LiDAR data and RGB images, and f) canopy diameter between LiDAR data and RGB images. Equal letters indicate no statistically significant difference, whereas different letters indicate a significant difference at the 5% level.

Based on the geostatistical analysis, all variables showed spatial dependence (Table 3; Fig. 5), with the degree of dependence ranging from moderate to strong. This condition was evidenced by the fitting of theoretical models to the semivariograms, in which semivariance increased with distance until reaching an approximately stable sill, indicating the existence of spatial structure and allowing the maximum distance of spatial influence of the observations to be estimated (Carvalho et al., 2013). In this study, the spherical model was adopted for all evaluated variables, with the fits verified by cross-validation. The choice of this model is consistent with previous geostatistical studies in coffee plantations, in which the spherical model was used to represent the spatial variability of plant attributes, such as plant height and canopy diameter (Carvalho et al., 2013; Ferraz et al., 2017).

Table 3. Parameters of the fitted semivariogram models for plant height and canopy diameter, with 95% confidence intervals estimated by jackknife and RMSE from cross-validation

Variable	Model	C0	C1	C0 + C1	A	A'	DSD	Class	RMSE
Field height	Spherical	154.37 [36.63 – 272.09]	62.76 [0.00 – 271.50]	217.13 [57.04 – 377.23]	91.92 [57.63 – 126.22]	91.92 [57.63 – 126.22]	71.09	Moderate	13.39 [9.15 – 17.63]
RGB height	Spherical	0.00 [0.00 – 0.00]	366.10 [183.01 – 549.20]	366.10 [183.01 – 549.20]	7.42 [6.28 – 8.55]	7.42 [6.28 – 8.55]	0.00	Strong	19.50 [14.60 – 24.40]
LiDAR height	Spherical	89.06 [28.88 – 149.24]	97.30 [0.00 – 256.24]	186.36 [48.42 – 324.30]	88.10 [62.96 – 113.25]	88.10 [62.96 – 113.25]	47.79	Moderate	10.66 [7.82 – 13.50]
Field canopy diameter	Spherical	0.00 [0.00 – 317.79]	305.64 [0.00 – 644.67]	305.64 [161.21 – 450.07]	6.95 [0.00 – 15.13]	6.95 [0.00 – 15.13]	0.00	Strong	17.70 [13.32 – 22.08]
RGB canopy diameter	Spherical	0.00 [0.00 – 530.47]	385.43 [0.00 – 985.00]	385.43 [94.93 – 675.92]	7.92 [0.00 – 16.11]	7.92 [0.00 – 16.11]	0.00	Strong	19.76 [11.74 – 27.78]
LiDAR canopy diameter	Spherical	0.00 [0.00 – 0.00]	272.06 [146.96 – 397.16]	272.06 [146.96 – 397.16]	7.58 [3.10 – 12.06]	7.58 [3.10 – 12.06]	0.00	Strong	16.66 [12.71 – 20.61]

The nugget effect was different from zero only for height obtained from field measurements and LiDAR, indicating the presence of variability not explained by the sampling grid and/or associated with short-scale components and measurement uncertainties (McBratney & Webster, 1986; Carvalho et al., 2013). In the remaining cases, the nugget effect was equal to zero, resulting in strong spatial dependence according to the DSD criterion.

The range represents the zone of influence of an observation, separating the structured domain, where samples are correlated, from the random domain, where samples

are independent (Andriotti, 2003; Carvalho et al., 2013). For height, the field and LiDAR data showed the largest ranges, with values of 91.92 m and 88.10 m, respectively.

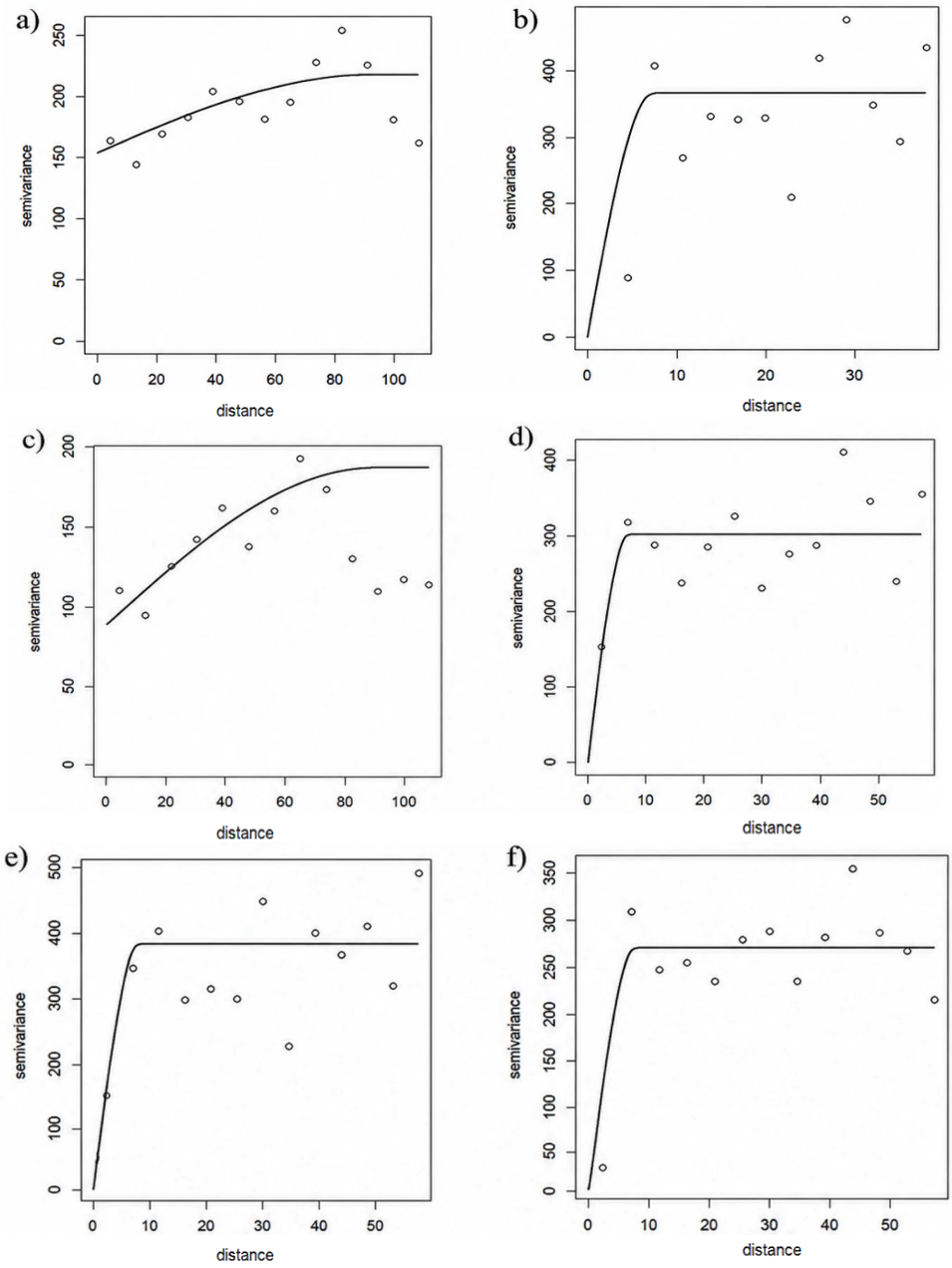

Figure 5. Semivariograms of: a) plant height from field data, b) plant height from RGB imagery, c) plant height from LiDAR data, d) canopy diameter from field data, e) canopy diameter from RGB imagery, and f) canopy diameter from LiDAR data.

These values were close to the maximum distance between sampling points (113 m), indicating broad spatial continuity. However, their interpretation should be approached with caution, since the uncertainty of variogram parameters tends to increase when the range is large relative to the extent of the sampling domain, due to the lower repetition of spatial structures within the evaluated area (Larocque et al., 2007). In contrast, the height estimated from RGB imagery showed a reduced range of 7.42 m, a value closer to the minimum distance between points, approximately 4 m, suggesting short-distance spatial dependence. This behavior may be associated with greater local variability in the photogrammetric reconstruction, since the quality and completeness of SfM-derived three-dimensional models are sensitive to acquisition conditions, image overlap, vegetation movement, and the structural complexity of the canopy (Frey et al., 2018). These limitations may introduce local variations in height estimates, reducing the spatial continuity of the variable. For canopy diameter, the ranges were reduced and similar among methods, varying from 6.95 m to 7.92 m, values close to the minimum distance between sampling points, 4 m. This pattern indicates short-distance spatial dependence, suggesting that diameter variability was predominantly controlled by local differences between plants.

The semivariogram sill (C0 + C1) represents the value at which semivariance tends to stabilize, indicating the maximum level of spatial variability modeled for the analyzed variable. When the semivariogram has a well-defined sill, this value is expected to be close to the sample variance of the data, since both express the overall variability of the variable (Webster & Oliver, 2007). In the present study, this comparison was performed between the C0 + C1 values presented in Table 3 and the sample variances described in Table 1. For canopy diameter, strong proximity between these values was observed for the three methods: field, with a sill of 305.64 cm² and variance of 305.22 cm²; RGB, with a sill of 385.43 cm² and variance of 386.76 cm²; and LiDAR, with a sill of 272.06 cm² and variance of 273.30 cm². For height, this relationship was more evident in RGB, whose sill was 366.10 cm², very close to the sample variance of 363.46 cm². In contrast, the field and LiDAR data showed sills higher than their respective sample variances, with 217.13 cm² versus 183.62 cm² for field data and 186.36 cm² versus 135.29 cm² for LiDAR. This behavior suggests lower correspondence between the modeled variability and the observed variability in the height fits obtained from field and LiDAR data.

Cross-validation indicated better predictive performance of LiDAR for both variables. For height, LiDAR showed the lowest RMSE (10.66 cm), followed by field data (13.39 cm) and RGB (19.50 cm). For canopy diameter, the same pattern was observed, with the lowest RMSE for LiDAR (16.66 cm), an intermediate value for field data (17.70 cm), and the highest error for RGB (19.76 cm). Thus, although RGB showed greater proximity between sill and variance for height, its higher RMSE values indicate greater predictive uncertainty in kriging, possibly associated with local variability and limitations in the photogrammetric reconstruction of the canopy (Frey et al., 2018).

After fitting the semivariogram for each coffee structural variable, it was possible to build spatial distribution (prediction) maps and the respective prediction standard-error maps for both variables, considering the three evaluated data sources as shown in Figs 6–7.

In the height maps (Fig. 6), ordinary kriging allowed the continuous spatial distribution of the variable to be estimated and, complementarily, local uncertainty to be quantified through the prediction standard error. This procedure is consistent with Carvalho et al.

(2013), who describe kriging as a step performed after semivariogram fitting to estimate values at unsampled locations, and with Ferraz et al. (2017), who used standard error maps to assess the reliability of interpolated values for coffee plant attributes.

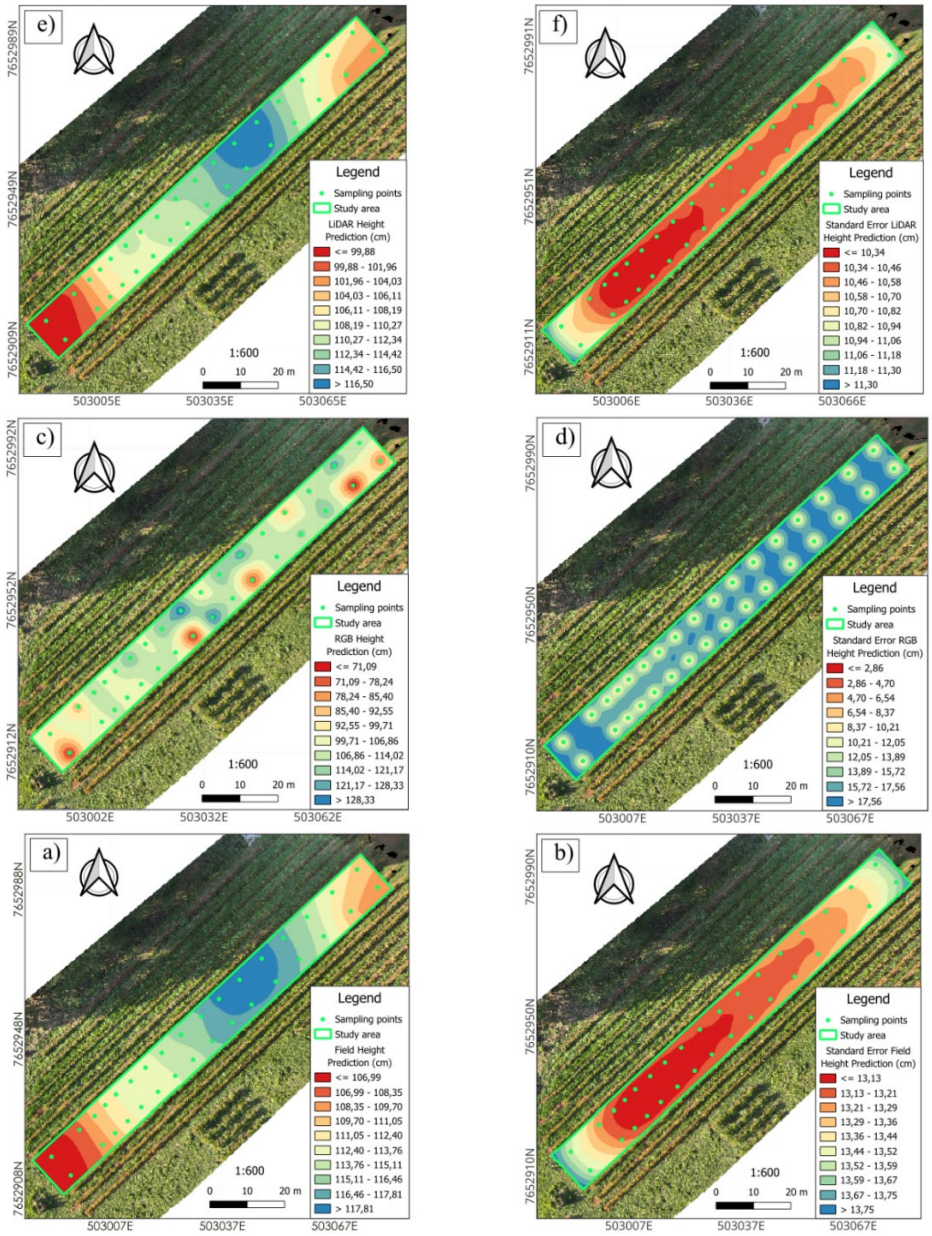

Figure 6. Spatial distribution maps of: a) plant height from field data, b) prediction standard error of plant height from field data, c) plant height from RGB imagery, d) prediction standard error of plant height from RGB imagery, e) plant height from LiDAR data, and f) prediction standard error of plant height from LiDAR data.

The surfaces obtained from field and LiDAR data (Fig. 6, a, e) showed more continuous patterns and broader spatial gradients, consistent with the larger ranges estimated for these methods, 91.92 m and 88.10 m, respectively. In contrast, the height estimated from RGB imagery (Fig. 6, c) showed a more localized distribution, with patches of high and low values more concentrated near the sampling points.

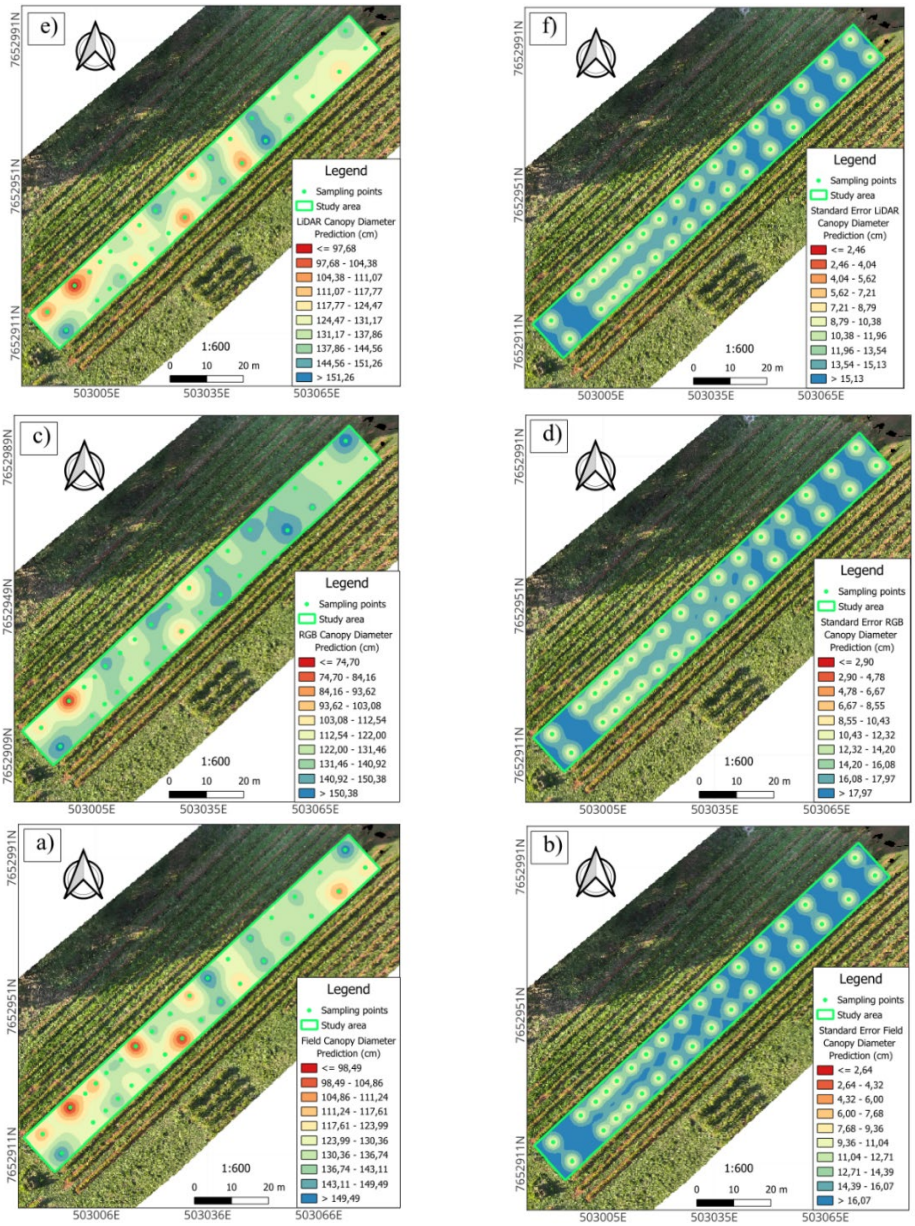

Figure 7. Spatial distribution maps of: a) canopy diameter from field data, b) prediction standard error of canopy diameter from field data, c) canopy diameter from RGB imagery, d) prediction standard error of canopy diameter from RGB imagery, e) canopy diameter from LiDAR data, and f) prediction standard error of canopy diameter from LiDAR data.

This behavior is associated with the short range of the RGB semivariogram, 7.42 m, a value close to the minimum distance between sampling points, indicating that the spatial influence of the observations was restricted to short distances. The standard error maps show greater uncertainty at the borders and lower error near the sampling points, a pattern explicitly reported for coffee plant attributes by Ferraz et al. (2017). This pattern was particularly evident for RGB (Fig. 6, d), whose short range resulted in error zones that were more clearly delimited around the sampled points, indicating a greater dependence of kriging on the immediate neighborhood of the samples.

For canopy diameter (Fig. 7), ordinary kriging also allowed the spatial distribution of the variable and the uncertainty associated with the predictions to be represented. However, unlike height, the canopy diameter maps (Fig. 7, a, c, e) showed more localized spatial transitions, with patches of higher and lower magnitude distributed in smaller zones. This behavior is consistent with the reduced ranges estimated for the three methods: 6.95 m for field data, 7.92 m for RGB, and 7.58 m for LiDAR. This characteristic was also reflected in the standard error maps (Fig. 7b, d, f), in which uncertainty was more marked between the points and at the borders of the area, while the lowest errors occurred near the sampling points, consistent with Ferraz et al. (2017).

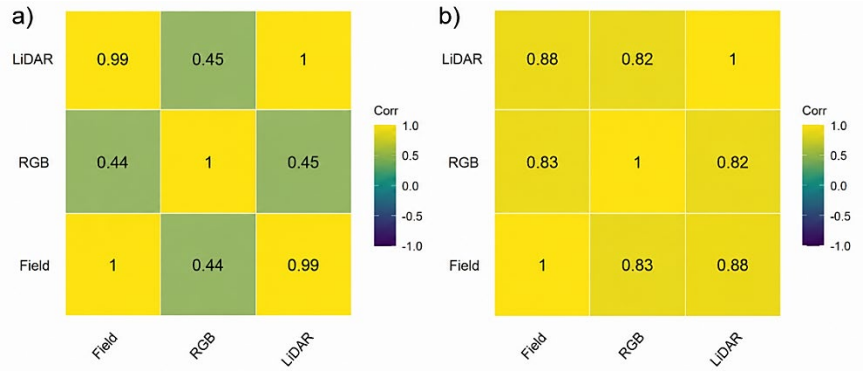

Figure 8. Correlation heatmaps between prediction maps of: a) plant height and b) canopy diameter.

The correlation heatmaps between kriged surfaces (Fig. 8) indicated high spatial agreement between LiDAR and field data for plant height ($r = 0.99$), whereas RGB showed a lower association with field data ($r = 0.44$) and with LiDAR ($r = 0.45$). For canopy diameter, the correlations were more balanced and higher among the methods, with $r = 0.88$ between LiDAR and field data, $r = 0.83$ between RGB and field data, and $r = 0.82$ between RGB and LiDAR. Correlations between maps tend to be higher than those obtained from point-based data because kriging produces estimates on a common grid and incorporates the spatial autocorrelation structure of the semivariogram, reducing the effect of local fluctuations and microscale noise. This effect is consistent with Souri et al. (2022), who discuss that direct comparisons between point measurements and gridded products assume homogeneity within the pixel and may induce non-physical discrepancies due to scale differences, making it more appropriate to compare fields on the same spatial support, pixel by pixel.

The error metrics calculated in the pixel-by-pixel comparison between the kriged maps (Table 4) indicated greater proximity of LiDAR to the field data compared with

RGB. For height, the comparison between LiDAR and field data resulted in lower ME (-4.150 cm) and lower RMSE (4.582 cm) than the comparison between RGB and field data (ME = -7.868 cm; RMSE = 11.981 cm). For canopy diameter, a similar behavior was observed, with lower errors in the comparison between LiDAR and field data (ME = 0.752 cm; RMSE = 4.436 cm) compared with the comparison between RGB and field data (ME = 1.854 cm; RMSE = 6.401 cm). The differences between LiDAR and RGB were more pronounced for height (RMSE = 9.793 cm) than for canopy diameter (RMSE = 6.329 cm), indicating greater divergence between the methods in representing the vertical structure of coffee plants.

Table 4. Error metrics from kriged map comparison and leave-one-out cross-validation (LOOCV) for plant height and canopy diameter obtained from RGB imagery, LiDAR, and field measurements

Comparison	Variable	ME maps (cm)	RMSE maps (cm)	ME LOOCV (cm)	RMSE LOOCV (cm)
RGB image vs. Field	Plant height	-7.868	11.981	-7.776	16.154
RGB image vs. Field	Canopy diameter	1.854	6.401	1.621	17.815
LiDAR vs. Field	Plant height	-4.150	4.582	-3.925	13.547
LiDAR vs. Field	Canopy diameter	0.752	4.436	0.738	17.614
LiDAR vs. RGB image	Plant height	-3.718	9.793	-3.768	12.713
LiDAR vs. RGB image	Canopy diameter	1.103	6.329	0.816	16.699

In the LOOCV validation, the RMSE values were higher than those obtained from the direct comparison between maps, indicating a more restrictive assessment of predictive performance. Even so, in relation to the field data, LiDAR showed lower bias and lower RMSE for height (ME = -3.925 cm; RMSE = 13.547 cm) and canopy diameter (ME = 0.738 cm; RMSE = 17.614 cm) when compared with RGB, which presented ME = -7.776 cm and RMSE = 16.154 cm for height, and ME = 1.621 cm and RMSE = 17.815 cm for canopy diameter. Therefore, the high correlation between the LiDAR and field maps should be analyzed together with the error metrics and the LOOCV validation, which confirm greater agreement between LiDAR and the reference measurements and lower relative performance of the estimates derived from RGB images.

The interpretation of the results also considers the experimental scope adopted, restricted to a specific cultivation and sampling condition. This characteristic may restrict direct extrapolation to larger commercial plantations, adult plants with more closed canopies, or different spacing and management systems. In this sense, evaluation in larger areas, different coffee plant ages, distinct canopy closure levels, and contrasting planting configurations may strengthen the applicability of the method.

In addition to broadening the evaluation conditions, the frequency of structural monitoring should be defined considering crop age and the expected rate of canopy change. In recently transplanted plants, monitoring may be carried out every three to four months during the establishment and vegetative growth stages, as reported by Bento et al. (2022). In adult coffee plantations, where structural changes tend to be more gradual, monitoring may be concentrated at specific phenological or management stages, such as pre-harvest, post-harvest, flowering, and fruit filling, following the multitemporal approach adopted by Martello et al. (2022).

Although the RPA platform used in this study integrated a thermal camera, only RGB information was employed to estimate structural variables. However, thermal data could complement the interpretation by indicating canopy temperature patterns associated with plant water status, whereas multispectral data could provide information on vigor and physiological condition through vegetation indices, extending the assessment beyond canopy dimensions.

CONCLUSIONS

It was possible to compare three approaches for obtaining coffee plant height and canopy diameter: manual field measurements, three-dimensional reconstruction from RGB images, and portable LiDAR with SLAM technology. The integration of geostatistics allowed the spatial dependence of the variables to be characterized, kriged maps to be generated, and the spatial coherence among the methods to be evaluated. LiDAR showed greater agreement with the field data, especially for plant height, with lower error and greater spatial continuity. RGB images showed lower performance, mainly for height; however, they allowed the structural variables to be estimated and their spatial distribution to be mapped, although with greater uncertainty and more localized patterns. Thus, the combination of point-based metrics, cross-validation, and geostatistical analysis provided a comprehensive assessment of coffee plant morphometric variables.

ACKNOWLEDGEMENTS. The authors thank CNPq (Projects No. 310186/2023-4, 444384/2024-3, 302584/2025-0 and 404462/2025), FAPEMIG (Project No. APQ-00661-22), and CAPES for financial support; Núcleo de Estudos em Sistemas Agrícolas (NESA); the Postgraduate Program in Agricultural Engineering; Universidade Federal de Lavras (UFLA); and Università degli Studi di Firenze (UniFI).

REFERENCES

Abreu, A.L., Ferraz, G.A.S., Morais, R., Bento, N.L., Conti, L., Bambi, G. & Ferraz, P.F.P. 2024. Use of geostatistical analyses for wheat production areas through the variables NDVI, surface temperature and yield. *Agronomy Research* **22**(S1), 329–345. https://doi.org/10.15159/AR.24.021

Almeida, A.Q.D, Souza, R.M.S., Siqueira e Silva, S.M., Oliveira, I.S.D, Cavalcante, F.D.S., & Melo, J.A.D.S. 2016. Space-time dependence of jatropha growth parameters grown in Brazilian semiarid. *Revista Caatinga* **29**(2), 358–366. https://doi.org/10.1590/1983-21252016v29n212rc

Álvares, C.A., Stape, J.L., Sentelhas, P.C., Moraes Gonçalves, J.L.D. & Sparovek, G.2013. Köppen's climate classification map for Brazil. *Meteorologische Zeitschrift* **22**(6), 711–728. https://doi.org/10.1127/0941-2948/2013/0507

Andriotti, J.L.S. 2003. *Fundamentals of statistics and geostatistics*. Unisinos, São Leopoldo, 165 pp. (in Portuguese).

Barbosa, B.D.S., Ferraz, G.A..S., Costa, L., Ampatzidis, Y., Vijayakumar, V. & Santos, L.M.D. 2021a. UAV-based coffee yield prediction utilizing feature selection and deep learning. *Smart Agricultural Technology* **1**, 1–9. https://doi.org/10.1016/j.atech.2021.100010

Barbosa, B.D.S., Ferraz, G.A.S., Santos, L.M.D., Santana, L.S., Marin, D.B., Rossi, G. & Conti, L. 2021b. Application of rgb images obtained by UAV in coffee farming. *Remote Sensing* **13**(12), 1–19. https://doi.org/10.3390/rs13122397

Bento, N.L., Ferraz, G.A.S., Barata, R.A.P., Soares, D.V., Santana, L.S. & Barbosa, B.D.S. 2022. Estimate and Temporal Monitoring of Height and Diameter of the Canopy of Recently Transplanted Coffee by a Remotely Piloted Aircraft System. *AgriEngineering* **4**(1), 207–215. https://doi.org/10.3390/agriengineering4010015

Bento, N.L., Ferraz, G.A.S., Santana, L.S., Faria, R.D.O., Rossi, G. & Bambi, G. 2025. Plant Height and Soil Compaction in Coffee Crops Based on LiDAR and RGB Sensors Carried by Remotely Piloted Aircraft. *Remote Sensing* **17**(8), 1–17. https://doi.org/10.3390/rs17081445

Bento, N.L., Ferraz, G.A..S., Santana, L.S. & Silva, M.D.L.O.e. 2023. Coffee Growing with Remotely Piloted Aircraft System: Bibliometric Review. *AgriEngineering* **5**(4), 2458–2477. https://doi.org/10.3390/agriengineering5040151

Bing, Q., Zhang, R., Zhang, L., Li, L. & Chen, L. 2025. UAV-SfM Photogrammetry for Canopy Characterization Toward Unmanned Aerial Spraying Systems Precision Pesticide Application in an Orchard. *Drones* **9**(2), 1–31. https://doi.org/10.3390/drones9020151

Cambardella, C.A., Moorman, T.B., Novak, J.M., Parkin, T.B., Karlen, D.L., Turco, R.F. & Konopka, A.E. 1994. Field-Scale Variability of Soil Properties in Central Iowa Soils. *Soil Science Society of America Journal* **58**(5), 1501–1511. https://doi.org/10.2136/sssaj1994.03615995005800050033x

Carvalho, L.C.C., Silva, F.M.D., Ferraz, G.A.S., Silva, F.C.D. & Stracieri, J.2012. Spatial variability of physical soil attributes and agronomic characteristics of coffee cultivation. *Coffee Science* **8**(3), 265–275 (in Portuguese).

Conab. 2025. *Monitoring the Brazilian coffee harvest: Fourth survey*. National Supply Company, Brasilia, 59 pp. (in Portuguese).

Cortes, A.F., Sampaio, A.P.L., Plazas, G.M.R., Costa, C.M.S.D., Montanari, R. & Oliveira, J.T.D. 2023. Spatial variability of dendrometric parameters in a native tree Mabea fistulifera Mart. and its relationship with soil physical properties. *Agronomia Colombiana* **41**(1), 1–11. https://doi.org/10.15446/agron.colomb.v41n1.103161

Dantas, A.A.A., Carvalho, L.G.D. & Ferreira, E. 2007. Climatic classification and tendencies in Lavras region, MG. *Ciênc. Agrotec* **31**(6), 1862–1866.

Diggle, P.J. & Ribeiro Jr., P.J. 2007. *Model-based geostatistics*. Springer, New York, 228 pp.

DJI. 2022. *DJI Mavic 3E/3T User Manual*. Shenzhen, 88 pp.

Escolà, A., Peña, J.M., López-Granados, F., Rosell-Polo, J.R., Castro, A.I.D., Gregorio, E., Jiménez-Brenes, F.M., Sanz, R., Sebé, F., Llorens, J. & Torres-Sánchez, J. 2023. Mobile terrestrial laser scanner vs. UAV photogrammetry to estimate woody crop canopy parameters – Part 1: Methodology and comparison in vineyards. *Computers and Electronics in Agriculture* **212**, 1–14. https://doi.org/10.1016/j.compag.2023.108109

Ferraz, G.A.S., Silva, F.M.D., Alves, M.S.C., Bueno, R.D.L. & Costa, P.A.N.D. 2012. Geostatistical analysis of fruit yield and detachment force in coffee. *Precision Agriculture* **13**, 76–89. https://doi.org/10.1007/s11119-011-9223-8

Ferraz, G.A.S., Silva, F.M.D., Oliveira, M.S.D., Custódio, A.A.P.D. & Ferraz, P.F.P. 2017. Spatial variability of plant attributes in a coffee plantation. *Revista Ciencia Agronomica* **48**(1), 81–91 (in Portuguese). https://doi.org/10.5935/1806-6690.20170009

Frey, J., Kovach, K., Stemmler, S. & Koch, B. 2018. UAV photogrammetry of forests as a vulnerable process. A sensitivity analysis for a Structure from Motion RGB-image pipeline. *Remote Sensing* **10**(6), 912. https://doi.org/10.3390/rs10060912

Frogbrook, Z.L., Oliver, M.A., Salahi, M. & Ellis, R.H. 2002. Exploring the spatial relations between cereal yield and soil chemical properties and the implications for sampling. *Soil Use and Management* **18**(1), 1–9. https://doi.org/10.1111/j.1475-2743.2002.tb00043.x

Geosun. 2022a. *Handheld LiDAR Scanning System GS-100G: Color Point Cloud with Highly Integrated Camera*. Wuhan, 3 pp.

Geosun. 2022b. *PointCloudCreater 2.0.46 – SLAM Colorized 3D Point Cloud Processing Tool*. Wuhan Geosun Navigation Technology Co., Ltd., Wuhan, China.

https://www.geosunlidar.com/sale-13575149-pointcloudcreater-2-0-46-slam-colorized-3d-point-cloud-processing-tool.html

Gomes, F. & Garcia, C.H. 2002. *Statistics applied to agronomic and forestry experiments*. FEALQ, Piracicaba, 305 pp. (in Portuguese). https://doi.org/10.37856/bja.v76i3.1314

Grego, C.R., Vieira, S.R. & Xavier, M.A. 2010. Spatial variability of some biometric attributes of sugarcane plants (variety iacsp93-3046) and its relation to physical and chemical soil attributes. *Bragantia* **69**, 107–119.

Kerry, R. & Oliver, M.A. 2007. Sampling requirements for variograms of soil properties computed by the method of moments and residual maximum likelihood. *Geoderma* **140**(4), 383–396. https://doi.org/10.1016/j.geoderma.2007.04.019

Larocque, G., Dutilleul, P., Pelletier, B. & Fyles, J.W. 2007. Characterization and Quantification of Uncertainty in Coregionalization Analysis. *Mathematical Geology* **39**, 263–288. https://doi.org/10.1007/s11004-007-9086-8

Maita, S.M., Quispe, K., Díaz-Chuquizuta, H., Rengifo Sanchéz, R., Mercado Chinchay, R., Cuevas Gimenez, J.P. & Solórzano, R. 2025. Soil spatial variability in high-yield Peruvian Amazon coffee: a geostatistical approach for precision fertilization. *Frontiers in Soil Science* **5**, 1–16. https://doi.org/10.3389/fsoil.2025.1701602

Marchant, B.P. & Lark, R.M. 2007. Robust estimation of the variogram by residual maximum likelihood. *Geoderma* **140**(1–2), 62–72. https://doi.org/10.1016/j.geoderma.2007.03.005

Martello, M., Molin, J.P., Angnes, G. & Acorsi, M.G. 2022. Assessing the Temporal and Spatial Variability of Coffee Plantation Using RPA-Based RGB Imaging. *Drones* **6**(10), 1–17. https://doi.org/10.3390/drones6100267

Matheron, G. 1962. *Treatise on Applied Geostatistics*, Volume I: Memoirs of the Bureau of Geological and Mining Research. Editions Technip **14**, 333 pp. (in French).

McBratney, A.B. & Webster, R. 1986. Choosing functions for semi-variograms of soil properties and fitting them to sampling estimates. *Journal of Soil Science* **37**, 617–639.

Mora-Pérez, G., Villagra-Mendoza, K. & Arriola-Valverde, S. 2025. Evaluation of the behavior of the humidity and vegetation index in a coffee crop using remote sensors with Unmanned Aerial Vehicles. *Revista Tecnología En Marcha* **38**(1), 63–76 (in Spanish). https://doi.org/10.18845/tm.v38i2.7133

Patterson, H.D. & Thompson, R. 1971. Recovery of inter-block information when block sizes are unequal. *Biometrika* **58**(3), 545–554. https://doi.org/10.1093/biomet/58.3.545

Pereira-Obaya, D., Cabo, C., Ordóñez, C. & Rodríguez-Pérez, J.R. 2024. A Handheld Laser-Scanning-Based Methodology for Monitoring Tree Growth in Chestnut Orchards. *Sensors* **24**(6), 1–13. https://doi.org/10.3390/s24061717

Pinedo, L.E., Ortega Quispe, K., Ccopi Trucios, D., Urquizo Barrera, J., Rios Chavarría, C., Pizarro Carcausto, S., Matos Calderon, D., Patricio Rosales, S., Rodríguez Cerrón, M., Ore Aquino, Z., Paz Monge, M. & Castañeda Tinco, I. 2025. Estimation of height and aerial biomass in Eucalyptus globulus plantations using UAV-LiDAR. *Trees, Forests and People* **19**, 1–12. https://doi.org/10.1016/j.tfp.2024.100763

Quispe, K., Hermoza, N., Mejia, S., Romero-Chavez, L.E., Ottos, E., Arce, A. & Solórzano Acosta, R. 2025. Spatial Analysis of Soil Acidity and Available Phosphorus in Coffee-Growing Areas of Pichanaqui: Implications for Liming and Site-Specific Fertilization. *Agriculture (Switzerland)* **15**(15), 1–28. https://doi.org/10.3390/agriculture15151632

R Development Core Team. 2025. *R: A Language and Environment for Statistical Computing*. R Foundation for Statistical Computing, Vienna, Austria. https://www.R-project.org/

Ribeiro Junior, P.J. & Diggle, P.J. 2001. GeoR: a package for geostatistical analysis. *R News* **1**(2), pp 15–18.

Santana, L.S., Ferraz, G.A.S., Marin, D.B., Barbosa, B.D.S., Santos, L.M.D., Ferraz, P.F.P., Conti, L., Camiciottoli, S. & Rossi, G. 2021a. Influence of flight altitude and control points in the georeferencing of images obtained by unmanned aerial vehicle. *European Journal of Remote Sensing* **54**(1), 59–71. https://doi.org/10.1080/22797254.2020.1845104

Santana, L.S., Ferraz, G.A.S., Teodoro, A.J. D.S., Santana, M.S., Rossi, G. & Palchetti, E. 2021b. Advances in precision coffee growing research: A bibliometric review. *Agronomy* **11**(8), 1–16. https://doi.org/10.3390/agronomy11081557

Santos, L.M.D, Ferraz, G.A.S., Barbosa, B.D.S., Diotto, A.V., Maciel, D.T. & Xavier, L.A.G. 2020. Biophysical parameters of coffee crop estimated by UAV RGB images. *Precision Agriculture* **21**(6), 1227–1241. https://doi.org/10.1007/s11119-020-09716-4

Santos, P.A.B. Schwerz, F.D., Carvalho, L.G.D., Baptista, V.B.D.S., Marin, D.B., Ferraz, G.A.S., Rossi, G., Conti, L. & Bambi, G. 2023. Machine Learning and Conventional Methods for Reference Evapotranspiration Estimation Using Limited-Climatic-Data Scenarios. *Agronomy* **13**(9), 1–21. https://doi.org/10.3390/agronomy13092366

Sanz-Ablanedo, E., Chandler, J.H., Rodríguez-Pérez, J.R. & Ordóñez, C. 2018. Accuracy of Unmanned Aerial Vehicle (UAV) and SfM Photogrammetry Survey as a Function of the Number and Location of Ground Control Points Used. *Remote Sensing* **10**(10), 1–19. https://doi.org/10.3390/rs10101606

Scalon, J.D. 2024. *Spatial data analysis with applications in R*. /*Análise de dados espaciais com aplicações em R*. Editora UFLA, Lavras, 275 pp. (in Portuguese).

Silva, S.A.D.S., Ferraz, G.A.S., Figueiredo, V.C., Volpato, M.M.L., Ferreira, D.D., Machado, M.L., Borges, F.E.D.M. & Conti, L. 2025. Integration of Field Data and UAV Imagery for Coffee Yield Modeling Using Machine Learning. *Drones* **9**(10), 1–25. https://doi.org/10.3390/drones9100717

Silva, S.A., Lima, J.S.S. & Bottega, E.L. 2013. Yield mapping of arabic coffee and their relationship with plant nutritional status. *Journal of Soil Science and Plant Nutrition* **13**(3), 556–564.

Souri, A.H., Chance, K., Sun, K., Liu, X. & Johnson, M.S. 2022. Dealing with spatial heterogeneity in pointwise-to-gridded-data comparisons. *Atmospheric Measurement Techniques* **15**(1), 41–59. https://doi.org/10.5194/amt-15-41-2022

Torres-Sánchez, J., Escolà, A., Castro, A.L.D., López-Granados, F., Rosell-Polo, J.R., Sebé, F., Jiménez-Brenes, F.M., Sanz, R., Gregorio, E. & Peña, J.M. 2023. Mobile terrestrial laser scanner vs. UAV photogrammetry to estimate woody crop canopy parameters – Part 2: Comparison for different crops and training systems. *Computers and Electronics in Agriculture* **212**, 1–10. https://doi.org/10.1016/j.compag.2023.108083

Wang, K., Zhou, J., Zhang, W. & Zhang, B. 2021. Mobile lidar scanning system combined with canopy morphology extracting methods for tree crown parameters evaluation in orchards. *Sensors (Switzerland)* **21**(2), 1–15. https://doi.org/10.3390/s21020339

Webster, R. & Oliver, M.A. 2007. *Geostatistics for Environmental Scientists*. Wiley, Chichester, 336 pp.

You, H., Tang, X., You, Q., Liu, Y., Chen, J. & Wang, F. 2023. Study on the Differences between the Extraction Results of the Structural Parameters of Individual Trees for Different Tree Species Based on UAV LiDAR and High-Resolution RGB Images. *Drones* **7**(5), 1–20. https://doi.org/10.3390/drones7050317

Yu, J., Xu, L., Shu, Q., Luo, S. & Xi, L. 2024. Spatial effects analysis of natural forest canopy cover based on spaceborne LiDAR and geostatistics. *Frontiers in Plant Science* **15**, 1–16. https://doi.org/10.3389/fpls.2024.1361297

Zhang, W., Qi, J., Wan, P., Wang, H., Xie, D., Wang, X. & Yan, G. 2016. An easy-to-use airborne LiDAR data filtering method based on cloth simulation. *Remote Sensing* **8**(6), 1–22. https://doi.org/10.3390/rs8060501